

## Intrinsic Transparent Conductors without Doping

Xiuwen Zhang,<sup>1</sup> Lijun Zhang,<sup>1,†</sup> John D. Perkins,<sup>2</sup> and Alex Zunger<sup>1,\*</sup>

<sup>1</sup>Renewable and Sustainable Energy Institute, University of Colorado, Boulder, Colorado 80309, USA

<sup>2</sup>National Renewable Energy Laboratory, Golden, Colorado 80401, USA

(Received 27 May 2015; published 23 October 2015)

Transparent conductors (TCs) combine the usually contraindicated properties of electrical conductivity with optical transparency and are generally made by starting with a transparent insulator and making it conductive via heavy doping, an approach that generally faces severe “doping bottlenecks.” We propose a different idea for TC design—starting with a metallic conductor and designing transparency by control of intrinsic interband transitions and intraband plasmonic frequency. We identify the specific design principles for three such prototypical intrinsic TC classes and then search computationally for materials that satisfy them. Remarkably, one of the intrinsic TC,  $\text{Ag}_3\text{Al}_{22}\text{O}_{34}$ , is predicted also to be a prototype 3D compounds that manifest natural 2D electron gas regions with very high electron density and conductivity.

DOI: 10.1103/PhysRevLett.115.176602

PACS numbers: 72.15.-v, 71.20.-b, 73.21.Ac, 78.20.-e

The functionality of transparency plus conductivity [1,2] lies at the center of many technological applications such as solar cells, touch-screen sensors, light emitting diodes, electronic papers, infrared or ultraviolet photo detectors, smart windows, and flat panel display [1–9], yet materials with such seemingly contraindicated properties are difficult to come by. The traditional strategy for searching for TCs has followed the path illustrated by the arrow in Fig. 1(a): start from a transparent insulator and find ways to make it conductive by doping it extensively without affecting its optical transparency [1–9]. Successful examples are very few and include electron doped ZnO, Sn-doped  $\text{In}_2\text{O}_3$ , and La-doped  $\text{SrGeO}_3$  for electron-conducting (*n*-type) TCs [3,4,7,8], as well as hole-doped  $\text{CuAlO}_2$  and K-doped  $\text{SrCu}_2\text{O}_2$  for hole-conducting (*p*-type) TCs [5,9]. The limiting factors are rooted in defect physics [10–12] and include difficult to fulfill requirements such as finding wide-gap insulators that can be amply doped without promoting carrier compensation or structural deformations.

In this Letter, we revisit the basic-physics design principles needed for transparent conductivity and find that a different, previously overlooked route, illustrated by the arrow in Fig. 1(b), may be possible—start from an opaque conductor that already has plenty of free carriers, then design optical transparency to realize an intrinsic (i.e., without intentional chemical doping) TC. However, not all bulk conductors will do; one needs to search for bulk metals that (a) have a sufficiently broad energy window in their electronic structure either below the Fermi energy  $E_F$  (for an *n*-type TC) or above  $E_F$  (for a *p*-type TC), so the interband transitions across the “energy window” will not obscure optical transparency, and (b) do not have a high plasma frequency ( $\omega_p$ ) [13] (such as  $\sim 15$  eV/ $\hbar$  for Al [13]) so the free carrier reflection will not limit transparency. If one can find metals that satisfy such conditions this would result in the interesting case of metallic conductivity in a transparent and pristine (undoped) crystal. This approach is applicable

to *bulk compounds* and, thus, is different from the approach of using ultrathin films of metallic materials that are transparent only when they are kept ultra thin [14–17].

The two conditions noted above can appear unusual and indeed materials satisfying them have, to our knowledge, not been deliberately searched before. Here, we illustrate the concept of intrinsic TC by discussing first simple, hypothetical structures of RbTe in the zinc blende structure and highly compressed crystalline silicon in the diamond structure, followed by realistic but more complex metallic ceramics reported as having been previously synthesized (but not characterized for conductivity or transparency) in the ICSD compilation of inorganic structures [18] as well as

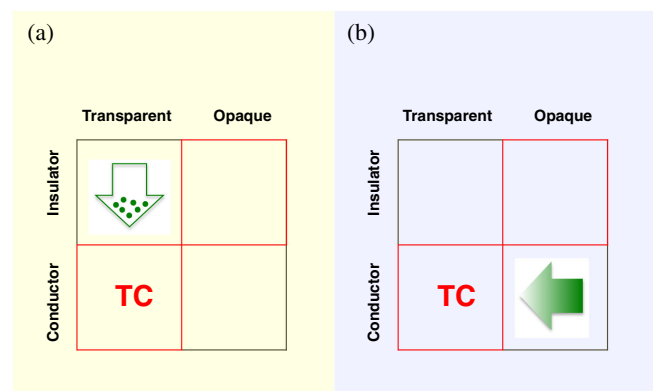


FIG. 1 (color online). (a) The traditional strategy for designing bulk transparent conductors that starts from a wide-gap insulator and finds ways to make it conductive by extensive doping without affecting its crystal structure or optical transparency. (b) The new strategy that starts from a metal that already has plenty of free carriers and designs optical transparency to realize an intrinsic (i.e., without intentional chemical doping) TC. This approach requires a technique for controlling the plasma frequency via the control of carrier density and band dispersion so the free carrier reflection will not limit transparency.

in specific literature on  $\text{Ag}_3\text{Al}_{22}\text{O}_{34}$  in the hexagonal  $P6_3/mmc$  structure [19] and  $\text{Ba}_3\text{Nb}_5\text{O}_{15}$  in the tetragonal  $P4/mbm$  structure [20]. In addition, using first principles thermodynamics based on DFT, we have computed their stability with respect to many possible competing phases, as described in the Supplemental Material, Sec. I [21]. Whereas these compounds, screened theoretically according to our design principles from hundreds of possibilities, are by no means optimized for maximal functionality, they clearly demonstrate the viability of the concept of intrinsic transparent conductors without doping. Remarkably, the free electrons predicted to exist in  $\text{Ag}_3\text{Al}_{22}\text{O}_{34}$  are found to be spatially organized as a *two dimensional electron gas (2DEG), periodically embedded in the 3D compound*.

To study the prototype behaviors of intrinsic transparent conductors, we evaluate their electronic structures, dielectric function, plasma frequency, and optical properties by the density functional theory (DFT) [22,23] as well as hybrid functional (HSE06) [24] (see Supplemental Material, Secs. II and III for details [21]).

*Type-1 intrinsic TC are metals with an isolated intermediate band.*—The first type (ITC-1) illustrated in Fig. 2 is based on metallic, intermediate-band (IB) materials where the IB is energetically isolated from the bands below and above it and the Fermi energy is located within that band. The particular example shown is based on RbTe in the zinc blende crystal structure [Fig. 2(a)] with electronic structure shown in Fig. 2(b).

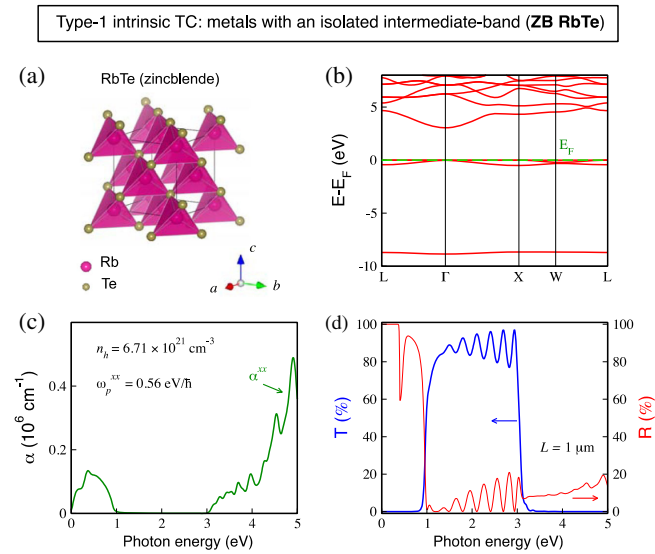


FIG. 2 (color online). (a) Crystal structure, (b) band structure, and (c) absorption coefficient ( $\alpha^{xx} = \alpha^{yy} = \alpha^{zz}$ ) of zinc blende ( $F-43m$ ) RbTe as an example of type-1 intrinsic TC from DFT. The carrier (hole) concentration ( $n_h$ ) and plasma frequency ( $\omega_p^{xx} = \omega_p^{yy} = \omega_p^{zz}$ ) are given in (c). The  $z$  axis is chosen along the [001] direction of the cubic lattice. (d) Transmission and reflection spectra of a freestanding  $1 \mu\text{m}$  thick RbTe ( $F-43m$ ) slab with optically smooth surfaces.

The *general* required design principles for this prototype (ITC-1) include the following. (i) The bands above the IB and the bands below IB need to be separated by broad energy windows from the IB [see, e.g., Fig. 2(b)] so as to prevent interband transitions by visible light photons. (ii) The energy spacing between different subbands within the IB needs to be smaller than visible light photon energy [Fig. 2(b)] so as to prevent intersubband transitions with visible-light frequencies. The way the narrowness of the IB helps to defeat intersubband absorption can also be used in conventional, chemically doped  $p$ -type TCs—such narrow bands could lead to high transparency, free of inter-valence-band transitions. (iii) The carrier density partially filling the IB needs to be in the region that gives a plasma frequency lower than the frequency of visible light but high enough for good conductivity [25]  $\sigma = [(\omega_p)^2/4\pi\gamma]$ , where  $\gamma$  is the damping coefficient [25] (we use  $\gamma = 0.2 \text{ eV}/\hbar$  analogous to traditional TCs [7]). The need to satisfy such multiple electronic structure functionalities is key to identification of such rare compounds. Fortunately, this is possible, as shown below.

Following these design principles, we focused our attention on the I–VI compounds (I = Rb and VI = Se, Te) in the zinc blende (ZB) structure, the reasons being that such suboctet I–VI compounds have a partially filled chalcogen  $p$  band that is energetically isolated from the alkali ion  $s$  bands above it and from the chalcogen ion  $s$  bands below it, thus forming a separate intermediate band [see, e.g., Fig. 2(b)]. Zinc blende RbTe is found to satisfy the conditions for ITC-1 rather well: the bulk optical absorption coefficient [Fig. 2(c)] including plasmonic effect based on Drude model [25] shows nearly zero optical absorption for most visible light. The plasma frequency [25]  $\omega_p \sim \sqrt{n_h/m^*}$  ( $0.56 \text{ eV}/\hbar$ ) is low enough for transparency due to the large effective mass  $m^*$  of IB, but high enough for good conductivity ( $0.21 \times 10^3 \text{ S/cm}$ ) due to the high hole density ( $n_h = Z/a^3 = 6.71 \times 10^{21} \text{ cm}^{-3}$ , where  $Z = 4$  is the number of holes in the unit cell and  $a = 8.42 \text{ \AA}$  is the calculated lattice constant). Indeed the simulated optical reflection and transmission spectra for a free standing  $1 \mu\text{m}$  thick slab with optically smooth surfaces [Fig. 2(d)] shows that the sample has very high transmittance ( $T$ ) and low reflectance ( $R$ ) for most visible light. Analogous results for ZB RbSe are shown in the Supplemental Material Fig. S4 [21]. However, we find that the ZB structure of RbTe (RbSe) is higher in energy than their  $\text{Na}_2\text{O}_2$ -type ground state structures [18] by  $0.655$  ( $0.701$ )  $\text{eV/atom}$ . We caution that in general the predicted intrinsic TC properties hold for the crystal structure and composition used in the prediction—other structures or compositions need not have the same ITC properties.

*Type-2 intrinsic TC is an indirect gap semimetal with large direct band gaps.*—The ITC-2 type is based on semimetals having a large *vertical* band gap (assuring optical transparency), yet a zero *indirect band gap*, assuring

semimetallic behavior. The particular example shown is based on compressed silicon in the diamond-type ( $Fd-3m$ ) structure [Fig. 3(a)] with DFT electronic structure calculations shown in Fig. 3(b).

The *general* required design principles for this prototype (ITC-2) include the following. (i) A large direct gap above the photon energy of most visible light between the ( $N_e$ )th and ( $N_e + 1$ )th bands ( $N_e$  is the number of electrons in the primitive cell) so the optical transition between them does not affect the transparency for visible light, and a zero indirect gap. This requires the ( $N_e$ )th and ( $N_e + 1$ )th bands to be highly dispersive and nearly parallel in a portion of the Brillouin zone [e.g., along the  $\Gamma$ - $X$  direction in Fig. 3(b)]. (ii) The carrier densities (equal amount of electrons and holes) need to be low enough to achieve a small plasma frequency and a weak optical transition of the electrons (holes) from the ( $N_e + 1$ )th [ $(N_e)$ th] band to higher (lower) bands.

Diamond-type ( $Fd-3m$ ) Si at high pressure (50 GPa) is chosen to illustrate the design principles although this structure is not the stable phase for highly compressed silicon (for pressure higher than  $\sim 11.2$  GPa, Si transforms [26] into the  $\beta$ -Sn  $I4_1/amd$  structure that is an opaque metal with calculated plasma frequency  $>9$  eV at pressures  $0 \sim 50$  GPa). Within this caveat, compressed Si is found to satisfy the conditions for ITC-2 rather well: the low carrier concentration ( $n = 0.08 \times 10^{21} \text{ cm}^{-3}$ ) leads to low plasma

frequency ( $0.58 \text{ eV}/\hbar$ ). Indeed the evaluated absorption coefficient [Fig. 3(c)] is nearly zero for most visible light and very small for infrared light. The transmittance [Fig. 3(d)] is mainly limited by the reflectivity that shows strong oscillatory pattern due to the coherent internal reflections. In actual technological applications, this can be largely mitigated through the use of antireflection coatings or optically rough surfaces.

*Type-3 intrinsic TC is a near-octet metal.*—The third type of intrinsic TC is based on metallic compounds that have a near-octet electronic structure. The particular example shown [Fig. 4(a)] is based on  $\text{Ag}_3\text{Al}_{22}\text{O}_{34}$  in the hexagonal  $P6_3/mmc$  structure [18] [inset of Fig. 4(b)]. Considering the standard formal charges of the constituents  $\text{Al}=3+$ ,  $\text{Ag}=1+$ , and  $\text{O}=2-$ , the compound  $\text{Ag}_3\text{Al}_{22}\text{O}_{34}$  would have  $1 \times 3 + 3 \times 22 - 2 \times 34 = +1$  nonzero residual valence per formula unit (the *net* physical charge is, however, zero as the nuclear charges compensate the electronic charges). Such near-octet compounds can be made, among other methods, by starting with wide gap octet insulator such as  $\text{Ca}_{12}\text{Al}_{14}\text{O}_{33}$  [6] and reducing it to  $\text{Ca}_{12}\text{Al}_{14}\text{O}_{32}$  [27], which is a metal. This example, tried previously [27], however, is not really transparent (see the Supplemental Material Fig. S5 [21]).

The *general* required design principles for this prototype (ITC-3) include the following. (i) The ( $N_e - \delta$ )th and ( $N_e - \delta + 1$ )th bands ( $N_e$  is the number of electrons and  $\delta$  is the residual valence per primitive cell) need to be

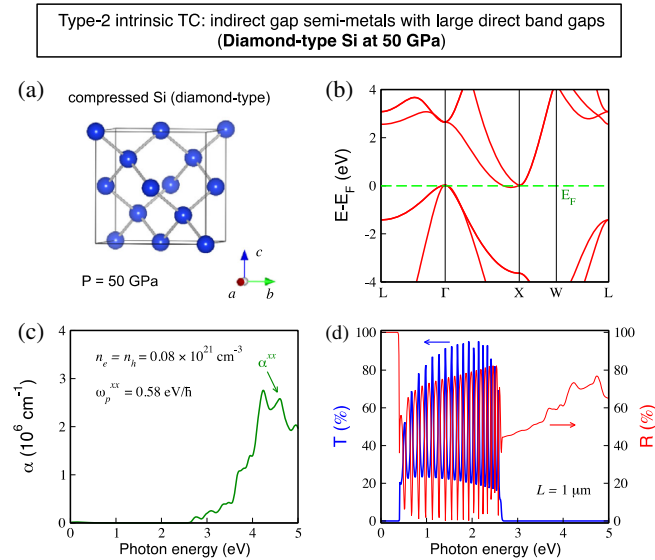


FIG. 3 (color online). (a) Crystal structure, (b) band structure, and (c) absorption coefficient ( $\alpha^{xx} = \alpha^{yy} = \alpha^{zz}$ ) of compressed diamond-type ( $Fd-3m$ ) Si under high pressure ( $P = 50$  GPa) as an example of type-2 intrinsic TC from DFT. The carrier (electron and hole) concentration ( $n_e = n_h$ ) and plasma frequency ( $\omega_p^{xx} = \omega_p^{yy} = \omega_p^{zz}$ ) are given in (c). The  $z$  axis is chosen along the  $[001]$  direction of the cubic lattice. (d) Transmission and reflection spectra of a free standing  $1 \mu\text{m}$  thick compressed Si ( $Fd-3m$ ) slab with optically smooth surfaces.

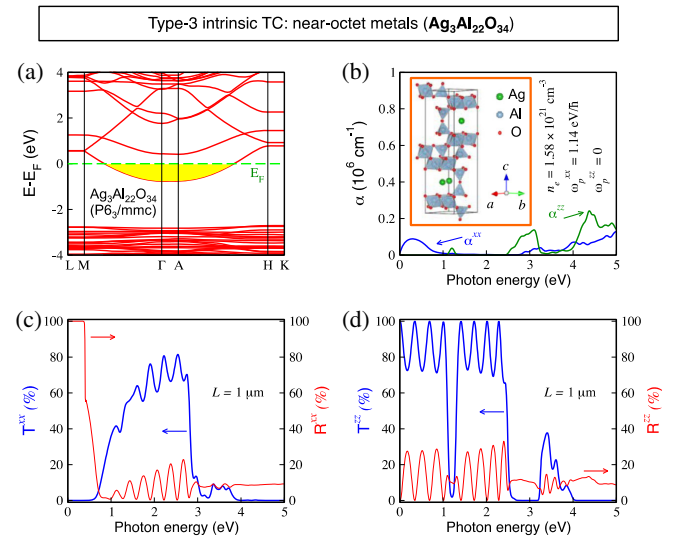


FIG. 4 (color online). (a) Band structure, (b) absorption coefficient ( $\alpha^{xx} = \alpha^{yy}$ ;  $\alpha^{zz}$ ) (inset: crystal structure) of  $\text{Ag}_3\text{Al}_{22}\text{O}_{34}$  ( $P6_3/mmc$ ) as an example of type-3 intrinsic TC from DFT. The yellow shading in (a) illustrates the electrons filling the band just below  $E_F$ . The carrier (electron) concentration ( $n_e$ ) and plasma frequency ( $\omega_p^{xx} = \omega_p^{yy}$ ;  $\omega_p^{zz}$ ) are given in (b). The  $z$  axis is chosen along the  $[0001]$  direction of the hexagonal lattice. (c)–(d) Transmission and reflection spectra of a free standing  $1 \mu\text{m}$  thick  $\text{Ag}_3\text{Al}_{22}\text{O}_{34}$  slab with optically smooth surfaces.



separated by a large energy window [see, e.g., Fig. 4(a)], so the interband optical transition across the energy window does not affect the transparency for visible light. (ii) The carrier density ( $n$ ) and dispersion of the partially filled bands [see Fig. 4(a)] need to be sufficiently low for low plasma frequency [25]  $\omega_p \sim \sqrt{n/m^*}$ . (iii) The optical transition of the electrons (holes) from the partially filled bands to the bands above (below) them needs to be weak so as not to adversely affect transparency.

Following the formulated design principles, we inspect a few hundreds of ternary oxides in ICSD [18], looking for near-octet residual valence  $|\delta| = 1$  (such as  $\text{Ag}_3\text{Al}_{22}\text{O}_{34}$  having  $\delta = 1$ ) with low carrier density. We readily identify two candidate ITC-3 materials:  $\text{Ag}_3\text{Al}_{22}\text{O}_{34}$  and  $\text{Ba}_3\text{Nb}_5\text{O}_{15}$ . Their thermodynamic stability is demonstrated in the Supplemental Material [21], Sec. I.  $\text{Ba}_3\text{Nb}_5\text{O}_{15}$  is found to be a stable ground state compound, whereas  $\text{Ag}_3\text{Al}_{22}\text{O}_{34}$  is slightly higher in energy (0.033 eV/atom) than its competing phases ( $\text{AgAlO}_2$ ,  $\text{Ag}$ , and  $\text{Al}_2\text{O}_3$ ). However,  $\text{Ag}_3\text{Al}_{22}\text{O}_{34}$  is found to satisfy the conditions for ITC-3 better than  $\text{Ba}_3\text{Nb}_5\text{O}_{15}$  (see the results of  $\text{Ba}_3\text{Nb}_5\text{O}_{15}$  in the Supplemental Material, Fig. S6 [21] analogous to the results of  $\text{Ag}_3\text{Al}_{22}\text{O}_{34}$  in Fig. 4) due to the deficit of energy bands near  $E_F$  in  $\text{Ag}_3\text{Al}_{22}\text{O}_{34}$  [see Fig. 4(a)]. The bulk optical absorption coefficient of  $\text{Ag}_3\text{Al}_{22}\text{O}_{34}$  [Fig. 4(b)] shows nearly zero absorption for most visible light, except the absorption peak near 3 eV for  $z$ -polarized light [see green curve in Fig. 4(b)] originating from the interband optical transitions from the partially filled band below  $E_F$  to the bands above  $E_F$ . The interplay between medium electron density ( $1.58 \times 10^{21} \text{ cm}^{-3}$ ) and medium band dispersion [see Fig. 4(a)] leads to small plasma frequencies ( $\omega_p^{xx} = \omega_p^{yy} = 1.14 \text{ eV}$ ). The calculated transmission spectrum of a  $1 \mu\text{m}$  thick slab [Figs. 4(c) and 4(d)] shows an overall transparency of  $\sim 70\%$ .

*Natural 2-dimensional electron gas (2DEG) forming in a 3D compound.*—Interestingly, we find that  $\text{Ag}_3\text{Al}_{22}\text{O}_{34}$  in the hexagonal  $P6_3/mmc$  crystal structure has very high in-plane ( $xy$ -plane) conductivity ( $\sigma^{xx} = [(\omega_p^{xx})^2/4\pi\gamma] = 0.88 \times 10^3 \text{ S/cm}$ ) but zero out-of-plane conductivity, *forming a 2DEG in a bulk compound* without the need for molecular beam epitaxy (MBE) synthesized heterostructures with designed modulation doping [28,29]. Another possible system [30]  $\text{Ca}_2\text{N}$ , does not have a truly 2D electron layer as, according to DFT, it has rather high out-of-plane conductivity (see the Supplemental Material Fig. S7 [21]) in comparison to the pure 2D conductivity in  $\text{Ag}_3\text{Al}_{22}\text{O}_{34}$  (Fig. 4). To demonstrate the distribution of carriers in intrinsic TC  $\text{Ag}_3\text{Al}_{22}\text{O}_{34}$ , we summed the charge density set up by wave functions in the energy region indicated by the yellow shading in Fig. 4(a) (between  $E_F - 1$  to  $E_F$  eV) and obtain the real space electron density shown in Fig. 5(a). We see that the two dimensional electron gas is confined primarily to the Ag-O layers and separated by the Al-O barriers [Fig. 5(a)]. The carrier density [Fig. 5(b)] of

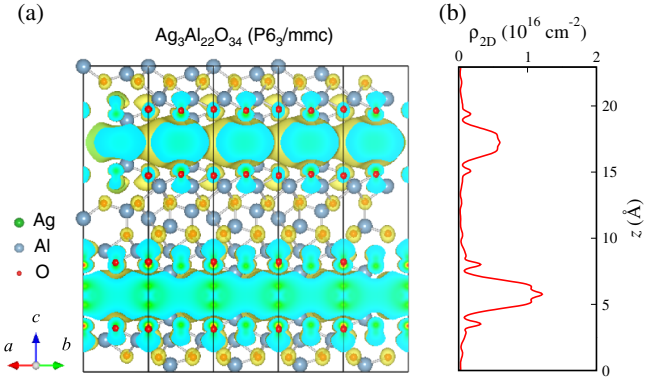


FIG. 5 (color online). (a) Real space electron density (isosurface  $0.5 \times 10^{21} \text{ cm}^{-3}$ ) of  $\text{Ag}_3\text{Al}_{22}\text{O}_{34}$  ( $P6_3/mmc$ ). (b) Two-dimensional carrier density in the  $xy$  plane as a function of the position  $z$ .

the 2DEG in the lower Ag-O region is about two times larger than that in the upper Ag-O layer, proportional to the number of Ag atoms [see inset of Fig. 4(b)]. As can be seen from the line plot in Fig. 5(b), the width at the half maximum of the 2DEG is 0.2–0.3 nm. Using this 2DEG thickness the carrier density in the lower Ag-O layer is as high as  $\sim 10^{16} \text{ cm}^{-2}$ —much higher density than the carrier density achieved in 2DEGs produced in MBE heterostructures ( $10^{11}$ – $10^{12} \text{ cm}^{-2}$  in semiconductor heterostructures and  $10^{13}$ – $10^{14} \text{ cm}^{-2}$  in oxide interfaces [29]). The carrier distribution in the intrinsic TCs could be significantly inhomogeneous as in the 2DEGs in Fig. 5. This will contribute to the dependence of  $\omega_p$  on the plasma wave vector  $q$ . In this study, we calculated  $\omega_p$  (described in the Supplemental Material, Sec. III [21]) for  $q = 0$ . This is appropriate when considering optical properties for visible light where the photon wave vector  $2\pi/\lambda$  (with wavelength  $\lambda$  of 390–700 nm) is considerably smaller than the zone-edge wave vector  $\pi/l$  of the unit cell with  $l$  being the lattice constant that is in the order of nm. We note that the spacing ( $\sim 1 \text{ nm}$ ) and periodicity ( $\sim 2 \text{ nm}$ ) of the alternating higher versus lower density 2DEGs are rather small; thus, the 2DEGs can couple with each other. This type of periodic high carrier-density 2DEGs in 3D compounds offers the route to study the mesoscopic collective effects of interacting periodic 2DEGs. The 2D conductivity of 2DEGs is also preferred for the high-performance 2D TC layers in devices for avoiding carrier scattering at the surfaces of TC layers.

*Conclusions.*—The strategy of designing TCs without deliberate doping [Fig. 1(b)] is a particular case of a broader approach of inverse design [11,31]—starting from physics based “design principles”, then constructing the “design metrics” that are computable quantities that embody the physics of the design principles, followed by extensive search of materials that score highly on the design metrics’ scale, leading to the identification of specific, few “best of class” materials. Here, we extend the initial step of inverse design by revisiting the basic design principles of a selected

functionality, leading us to the potentially overlooked prototypes of functional materials, such as the bulk compounds that support free carriers without extrinsic doping while maintaining transparency predicted in this study. Avoidance of deliberate doping [compare Fig. 1(a) with 1(b)] may circumvent structural defects and could thus simplify the manufacturing techniques compared to processes that rely on heavy, and often nonequilibrium doping. Indeed, a more extended search of these functionalities, in parallel with stability and growability calculations (exemplified by Fig. S1 in the Supplemental Material [21], which includes Refs. [32–35]) along with experimental scrutiny of such results might well be the way to accelerated discovery of functional materials.

This work was supported by the U.S. Department of Energy, Office of Science, Basic Energy Sciences, Materials Sciences and Engineering Division under Grant No. DE-FG02-13ER46959 to C.U. We thank Liping Yu and Giancarlo Trimarchi for helpful discussions. This work used resources of the National Energy Research Scientific Computing Center, which is supported by the Office of Science of the U.S. Department of Energy under Contract No. DE-AC02-05CH11231.

\*Corresponding author.

alex.zunger@colorado.edu

†Present address: College of materials science and Engineering, Jilin University, Changchun 130012, China.

- [1] D. S. Ginley, H. Hosono, and D. C. Paine, *Handbook of Transparent Conductors* (Springer Science & Business Media, New York, 2010).
- [2] A. V. Moholkar, *Transparent Conductors* (AV Akademiker-verlag GmbH & Co. KG, Saarbrücken, 2011).
- [3] K. Wasa, S. Hayakawa, and T. Hada, Electrical and optical properties of sputtered n-p ZnO–Si heterojunctions, *Jpn. J. Appl. Phys.* **10**, 1732 (1971).
- [4] I. Hamberg, A. Hjortsberg, and C. G. Granqvist, High quality transparent heat reflectors of reactively evaporated indium tin oxide, *Appl. Phys. Lett.* **40**, 362 (1982).
- [5] H. Kawazoe, M. Yasukawa, H. Hyodo, M. Kurita, H. Yanagi, and H. Hosono, P-type electrical conduction in transparent thin films of CuAlO<sub>2</sub>, *Nature (London)* **389**, 939 (1997).
- [6] K. Hayashi, S. Matsuishi, T. Kamiya, M. Hirano, and H. Hosono, Light-induced conversion of an insulating refractory oxide into a persistent electronic conductor, *Nature (London)* **419**, 462 (2002).
- [7] G. V. Naik, J. Kim, and A. Boltasseva, Oxides and nitrides as alternative plasmonic materials in the optical range, *Opt. Mater. Express* **1**, 1090 (2011).
- [8] H. Mizoguchi, T. Kamiya, S. Matsuishi, and H. Hosono, A germanate transparent conductive oxide, *Nat. Commun.* **2**, 470 (2011).
- [9] A. Kudo, H. Yanagi, H. Hosono, and H. Kawazoe, SrCu<sub>2</sub>O<sub>2</sub>: A p-type conductive oxide with wide band gap, *Appl. Phys. Lett.* **73**, 220 (1998).
- [10] Ç. Kılıç and A. Zunger, Origins of Coexistence of Conductivity and Transparency in SnO<sub>2</sub>, *Phys. Rev. Lett.* **88**, 095501 (2002).
- [11] T. R. Paudel, A. Zakutayev, S. Lany, M. d’Avezac, and A. Zunger, Doping rules and doping prototypes in A<sub>2</sub>BO<sub>4</sub> spinel oxides, *Adv. Funct. Mater.* **21**, 4493 (2011).
- [12] G. Hautier, A. Miglio, G. Ceder, G.-M. Rignanese, and X. Gonze, Identification and design principles of low hole effective mass p-type transparent conducting oxides, *Nat. Commun.* **4**, 2292 (2013).
- [13] E. D. Palik, *Handbook of Optical Constants of Solids* (Academic Press, Boston, 1998).
- [14] K. S. Kim, Y. Zhao, H. Jang, S. Y. Lee, J. M. Kim, K. S. Kim, J.-H. Ahn, P. Kim, J.-Y. Choi, and B. H. Hong, Large-scale pattern growth of graphene films for stretchable transparent electrodes, *Nature (London)* **457**, 706 (2009).
- [15] T. Ohsawa, J. Okubo, T. Suzuki, H. Kumigashira, M. Oshima, and T. Hitosugi, An n-Type transparent conducting oxide: Nb<sub>12</sub>O<sub>29</sub>, *J. Phys. Chem. C* **115**, 16625 (2011).
- [16] J. van de Groep, P. Spinelli, and A. Polman, Transparent conducting silver nanowire networks, *Nano Lett.* **12**, 3138 (2012).
- [17] X. Meng, D. Liu, X. Dai, H. Pan, X. Wen, L. Zuo, and G. Qin, Novel stable hard transparent conductors in TiO<sub>2</sub>-TiC system: Design materials from scratch, *Sci. Rep.* **4**, 7503 (2014).
- [18] Inorganic Crystal Structure Database, Fachinformationszentrum Karlsruhe, Germany, (2006).
- [19] W. A. England, A. J. Jacobson, and B. C. Tofield, Structural studies of highly non-stoichiometric polycrystalline sodium and silver beta-aluminas, *Solid State Ionics* **6**, 21 (1982).
- [20] B. Hessen, S. A. Sunshine, T. Siegrist, A. T. Fiory, and J. V. Waszczak, Structure and properties of reduced barium niobium oxide single crystals obtained from borate fluxes, *Chem. Mater.* **3**, 528 (1991).
- [21] See Supplemental Material at <http://link.aps.org/supplemental/10.1103/PhysRevLett.115.176602>, for detailed description of methodologies on thermodynamic stability, electronic structure, and optical property evaluation along with their application and testing.
- [22] J. P. Perdew, K. Burke, and M. Ernzerhof, Generalized Gradient Approximation Made Simple, *Phys. Rev. Lett.* **77**, 3865 (1996).
- [23] G. Kresse and D. Joubert, From ultrasoft pseudopotentials to the projector augmented-wave method, *Phys. Rev. B* **59**, 1758 (1999).
- [24] J. Heyd, G. E. Scuseria, and M. Ernzerhof, Hybrid functionals based on a screened Coulomb potential, *J. Chem. Phys.* **118**, 8207 (2003).
- [25] P. Drude, Zur Elektronentheorie der Metalle, *Ann. Phys. (Berlin)* **306**, 566 (1900).
- [26] J. Z. Hu and I. L. Spain, Phases of silicon at high pressure, *Solid State Commun.* **51**, 263 (1984).
- [27] S. Matsuishi, Y. Toda, M. Miyakawa, K. Hayashi, T. Kamiya, M. Hirano, I. Tanaka, and H. Hosono, High-Density electron anions in a nanoporous single crystal: [Ca<sub>24</sub>Al<sub>28</sub>O<sub>64</sub>]<sub>4+</sub> + (4e<sup>-</sup>), *Science* **301**, 626 (2003).
- [28] R. Dingle, H. L. Störmer, A. C. Gossard, and W. Wiegmann, Electron mobilities in modulation-doped semiconductor heterojunction superlattices, *Appl. Phys. Lett.* **33**, 665 (1978).

- [29] J. Mannhart and D.G. Schlom, Oxide interfaces—an opportunity for electronics, *Science* **327**, 1607 (2010).
- [30] K. Lee, S. W. Kim, Y. Toda, S. Matsuishi, and H. Hosono, Dicalcium nitride as a two-dimensional electride with an anionic electron layer, *Nature (London)* **494**, 336 (2013).
- [31] A. Franceschetti and A. Zunger, The inverse band-structure problem of finding an atomic configuration with given electronic properties, *Nature (London)* **402**, 60 (1999).
- [32] V. Stevanovic, S. Lany, X. Zhang, and A. Zunger, Correcting density functional theory for accurate predictions of compound enthalpies of formation: Fitted elemental-phase reference energies, *Phys. Rev. B* **85**, 115104 (2012).
- [33] R. Gautier, X. Zhang, L. Hu, L. Yu, Y. Lin, T.O.L. Sunde, D. Chon, K.R. Poeppelmeier, and A. Zunger, Prediction and accelerated laboratory discovery of previously unknown 18-electron ABX compounds, *Nat. Chem.* **7**, 308 (2015).
- [34] X. Zhang, L. Yu, A. Zakutayev, and A. Zunger, Sorting stable versus unstable hypothetical compounds: The case of multi-functional ABX half-heusler filled tetrahedral structures, *Adv. Funct. Mater.* **22**, 1425 (2012).
- [35] S. L. Dudarev, G. A. Botton, S. Y. Savrasov, C. J. Humphreys, and A. P. Sutton, Electron-energy-loss spectra and the structural stability of nickel oxide: An LSDA + U study, *Phys. Rev. B* **57**, 1505 (1998).